Macromolecules

pubs.acs.org/Macromolecules Article

Highly Enhanced Mechanical Strength and Toughness of Biodegradable PBAT Plastics through a Biobased Multiple Hydrogen Bonding Strategy

Zhi-Xiong Fei,[§] Jingrui Sun,[§] Chang Cui, Chenxiao Yin, Rui Zhan, Ling-Ying Shi,* Ke-Ke Yang,* and Yu-Zhong Wang*

Cite This: *Macromolecules* 2024, 57, 7043−7051 Read Online

ACCESS | Metrics & More | Article Recommendations | Supporting Information

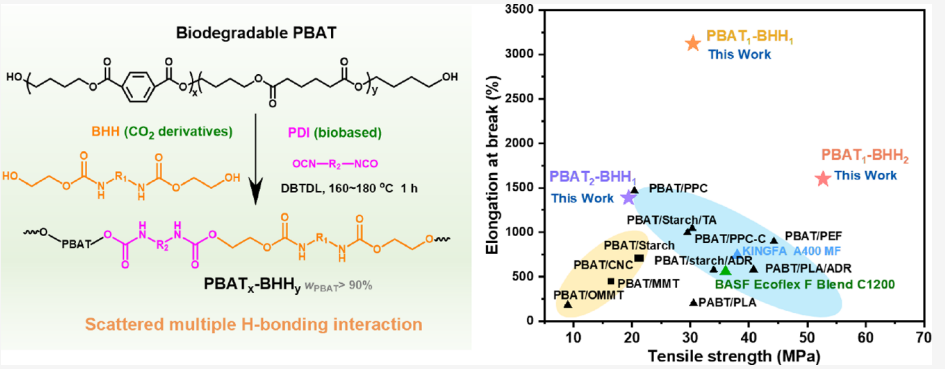

ABSTRACT: Poly(butyleneadipate-*co*-terephthalate) (PBAT), a favorable biodegradable polyester, exhibits striking application potential as a sustainable alternative of conventional petrochemical plastics to relieve the problems on environmental pollution. However, the utilization of PBAT materials is still limited due to their suboptimal strength and toughness. Here, we utilized melting chain extension reaction to incorporate multiple hydrogen bonding units into the main chain of PBAT, achieving the great enhancement in mechanical strength and toughness of the PBAT plastics. Melting copolymerization between the low-molecular-weighted (MW) PBAT and the biobased isocyanate- and carbon dioxide-derived bis(hydroxyalkyl carbamate) displays high effectivity and scalability, and the copolymerized PBAT presents highly enhanced mechanical performance (strength high up to 52 MPa, elongation at break >1500%, and fracture toughness high up to 583 MJ/m^3) much better than the commercial available high-MW PBAT and its composites, emphasizing its great potential to broaden the use of biodegradable PBAT in plastic products. We investigated the influence of the hard segment content on the mechanical and rheological behaviors and revealed the strengthening and toughening mechanisms. This work provides insights and scalable strategies for the development of high-performance biodegradable polyesters.

INTRODUCTION

Wide application of conventional plastics in domestic and industrial production causes growing plastic waste and serious environmental problems. According to the global analysis of the plastic waste generation trends throughout the entire history, approximately 5000 million metric tons (Mt) of waste plastics had been discarded in landfills or the natural environment in 2016, and it was predicted to be 12,000 Mt in 2050.[1] Most of the commodity plastics are from petroleum-originated polyolefin plastics, such as polypropylene, polyethylene, and polyvinyl chloride, which are not biodegradable after service life, leading to the "white pollution" and vast plastic debris entering into major ocean basins and marine environment.[2−5] Developing and utilizing biodegradable polymers as the alternatives have become an upswing desirable end-of-life option to combat these problems,[6−9] because they can be ultimately converted into carbon dioxide, water, and biomass under appropriate biologically active conditions after their intended use.

Poly(butylene adipate-*co*-terephthalate) (PBAT) is one typical fully biodegradable aliphatic-aromatic copolyester made of terephthalic acid (TPA), 1,4-butanediol, and adipic acid.[10,11] Compared to other biodegradable polyesters such as polylactic acid (PLA)[12,13] and polybutylene succinate (PBS),[14]

Received: May 21, 2024
Revised: July 7, 2024
Accepted: July 10, 2024
Published: July 22, 2024

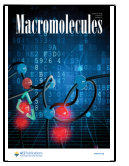

https://doi.org/10.1021/acs.macromol.4c01153
Macromolecules 2024, 57, 7043−7051

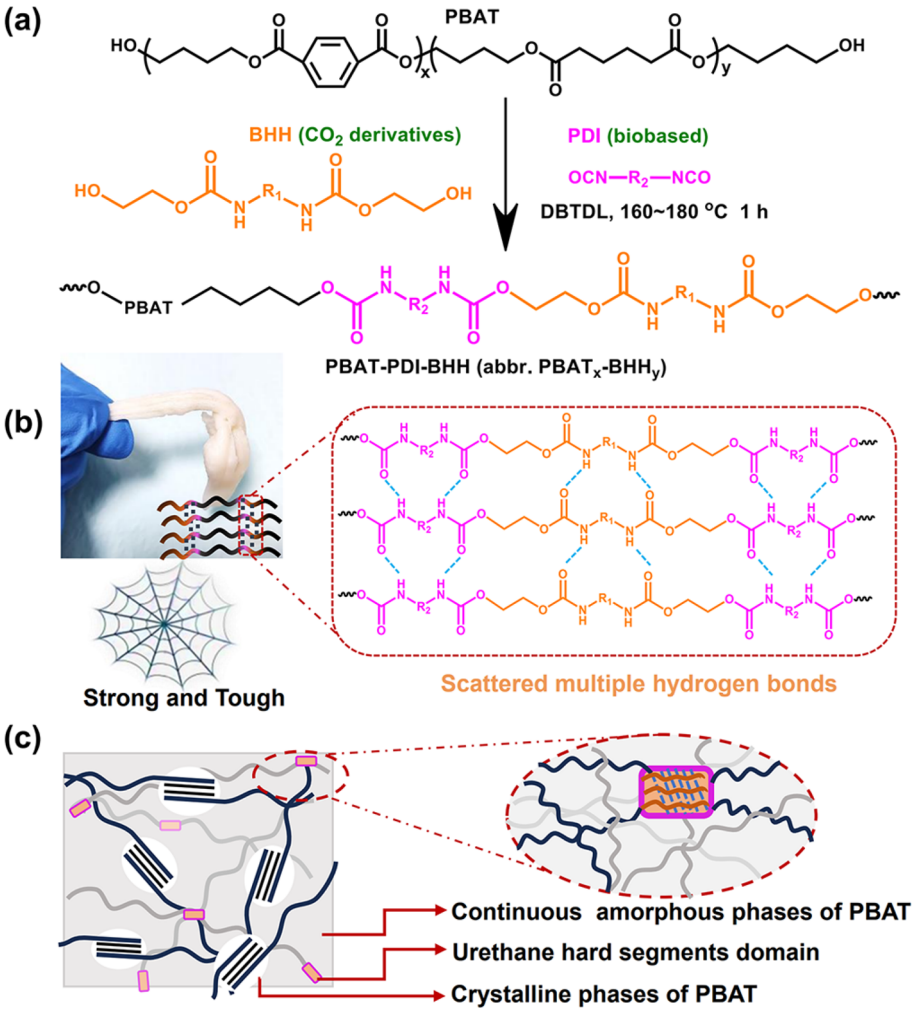

Figure 1. (a) Synthetic route of modified PBAT (R_1 = $(CH_2)_6$ and R_2 = $(CH_2)_5$) and schematic illustration of hydrogen bonding array (b) and microstructure (c) of $PBAT_x$-BHH_y for achieving strong strength and high toughness.

PBAT exhibits notable advantages including excellent flexibility with an elongation at break high up to 700% and complete biodegradability under mild climatic conditions.[15,16] PBAT with the trademark of Ecoflex provided by BASF designed for film extrusion and extrusion coating can be completely degraded within 5 months under landfilling[17] and has large importance in the market of biodegradable single-use packaging plastics and agricultural mulch films similar to LDPE.[18,19] Nevertheless, the relatively weak mechanical strength (<24 MPa)[9] of PBAT restricts its applications. To enhance the mechanical strength, many efforts have been conducted on blending PBAT with strong and brittle biodegradable polymers or biopolymers and nanoparticles such as polylactic acid (PLA),[20−23] poly(propylene carbonate) (PPC),[24,25] poly(ethylene 2,5-furanoate) (PEF),[26] starch,[27,28] cellulose nanocrystals (CNCs),[29] and organoclay.[30,31] However, the high melting viscosity of PBAT and the high immiscibility between PBAT and these additives have been the major limitations in the purpose of simultaneously improving the mechanical strength and toughness with the feasible processing ability.

In both nature and synthesized systems, unusual mechanical properties can be programmed by the combination of secondary supramolecular interactions such as hydrogen bonding, host−guest interaction, metal−ligand coordination, etc., for example, spider silk possesses ultrahigh tensile strength and toughness due to the multiple H-bonding interaction in the β-sheet nanocrystals.[32,33] The introduction of supramolecular interaction in the polyurethanes (PUs) has been demonstrated with great improvement of the mechanical strength and toughness with intrinsic self-healing and reprocessing capabilities.[34−37] In particular, the hydrogen bonding units with the bond strengths depending on the nature of donors and acceptors are commonly employed to construct high-performance PUs, while many multiple hydrogen bonding units are biobased and eco-friendly, such as the biourea-based ureido-pyrimidinone (UPy)[34,35,38] and carbon dioxide-derived carbonate diols.[39,40] The multiple hydrogen bonding interaction can greatly increase the mechanical strength, whereas the externally induced dynamic hydrogen bonding breakage and recombination can dissipate a large amount of energy, leading to high toughness. For example, the toughness of degradable PLA and cellulose was improved by hydrogen bonding interaction modification.[41,42] However, the supramolecular H-bonding interactions have not been induced into the main chain of PBAT to prepare homogeneous copolymer plastics for enhancing mechanical performance and durability.

In this work, we show the strategy of incorporating multiple H-bonding units into PBAT through the melting chain extension polymerization technique to achieve a strengthening

https://doi.org/10.1021/acs.macromol.4c01153
Macromolecules 2024, 57, 7043−7051

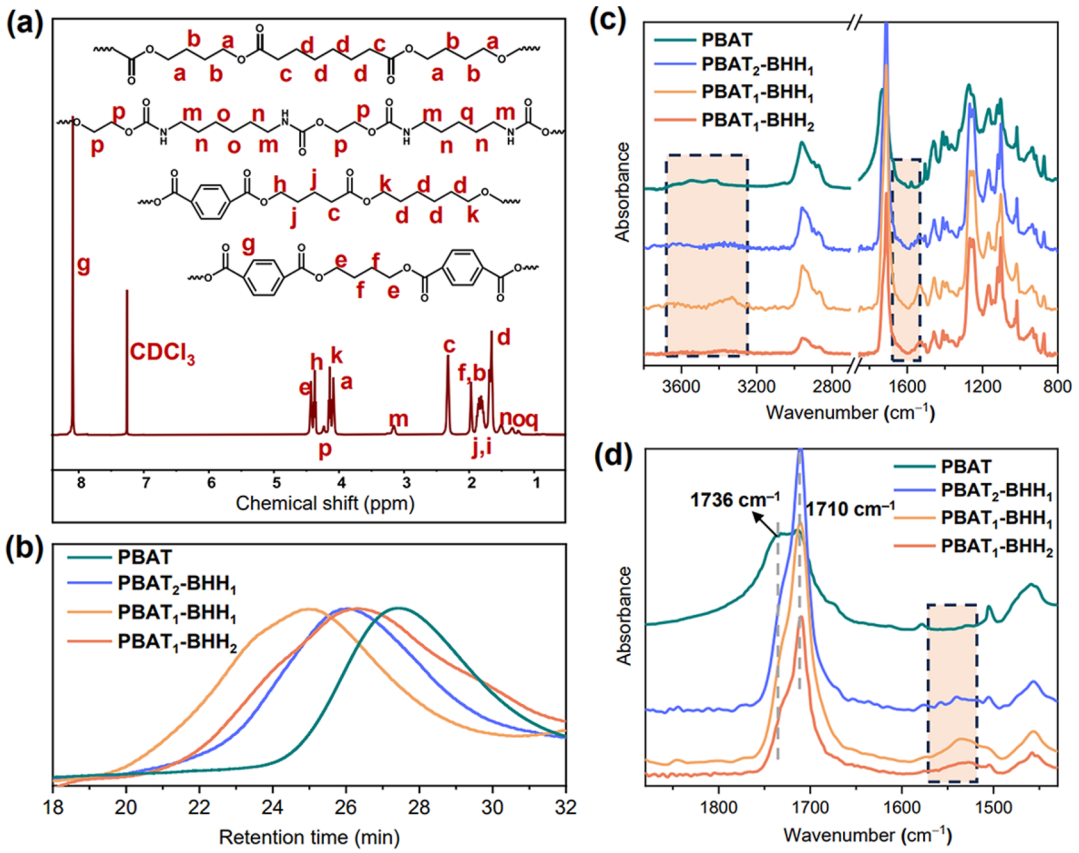

Figure 2. (a) ^{1}H NMR spectrum of PBAT$_1$-BHH$_1$ and (b) GPC curves and (c, d) FT-IR spectra of PBAT and PBAT$_x$-BHH$_y$.

and toughening mechanism. Bis(hydroxyalkyl carbamate)s derived from CO_2-based ethylene carbonate and α,ω-diamines were copolymerized with the low-molecular-weighted PBAT using the biobased 1,5-pentamethylene diisocyanate (PDI) chain extender through one-step melting polymerization. The resulted materials with a mass ratio of PBAT >90% present the extremely enhanced mechanic strength (up to 52 MPa), flexibility (~3000%), and toughness (~583 MJ/m^3). The greatly improved mechanical properties not only broaden the potential applications of PBAT but also make it a strong contender for further replacing traditional polyolefin materials.

RESULTS AND DISCUSSION

The chain extension reaction of PBAT diols (M_n ~ 10 kg mol^{-1}) with pentamethylene diisocyanate (PDI) and 1,6-bis(hydroxy-ethyloxy-carbonylamino) hexane (BHH) was carried out through a one-pot melting copolymerization process in the presence of dibutyltin dilaurate (DBTDL). The synthetic route is presented in Figure 1a (described in detail in the Supporting Information), and the hydrogen bonding interaction among polymer chains is illustrated in Figure 1b,c. PDI is a commercially available biobased diisocyanate, and BHH was synthesized from hexamethylene-diamine and ethylene carbonate derived from CO_2 according to a reported method (Figures S1−S3).[39,40] The chain extension reaction was performed under vacuum at 160−180 °C for only less than 3 h. The melting point of BHH is 95 °C, which is close to and slightly lower than T_m of raw PBAT, and thus, the stability and mobility of BHH ensure the homogeneity of PBAT/BHH mixture for the highly efficient reaction. We attempted directly incorporating different ratios of BHH into the copolymer by setting the mole ratio of PBAT and BHH at 1:2, 1:1, and 1:2 (Table S1), and the resulted products were noted as PBAT$_x$-BHH$_y$ (where x and y refer to the molar ratios of PBAT and BHH). In these PBAT$_x$-BHH$_y$, the weight fraction of PBAT (w_{PBAT}) is higher than 90% to ensure the biodegradability. The chemical structure of the copolymer was investigated by ^{1}H NMR spectroscopy (Figure 2a and Figure S4). The peaks with tags "m, n, o, q" represent the signal of CH_2 of the chain extender in Figure 2a and prove the successful introduction of PDI and BHH in the materials. The number-average molecular weights of PBAT-BHH copolymers ranged from 25 to 45 kg mol^{-1} with the polydispersity ($Đ$) value ~2.2, which were much higher than 7.8 kg mol^{-1} of parent PBAT from the gel permeation chromatography (GPC) results (Figure 2b and Table S1), indicating the successful chain extension reaction.

The FT-IR spectra in Figure 2c further confirm the successful chain extension reaction. The chain expansion reaction between −NCO and −OH was confirmed by the disappearance of the O−H stretching vibration peaks on PBAT at 3400−3600 cm^{-1} and the appearance of the N−H stretching vibration peaks near 3350 cm^{-1} and the N−H bond bending vibration peaks at 1540 cm^{-1}. The carbonyl peaks in the range of 1600−1850 cm^{-1} can be divided into two peaks centered at 1710 and 1736 cm^{-1}, which belong to hydrogen-bonded carbonyl and free carbonyl, respectively (Figure 2d). After the chain expansion reaction, the peak intensity at 1710 cm^{-1} increased dramatically, demonstrating that the statistical incorporation of BHH segments into PBAT induces significant improvement of hydrogen bonding interaction. Through peak fitting, the hydrogen-bonded carbonyl group increased

https://doi.org/10.1021/acs.macromol.4c01153
Macromolecules 2024, 57, 7043−7051

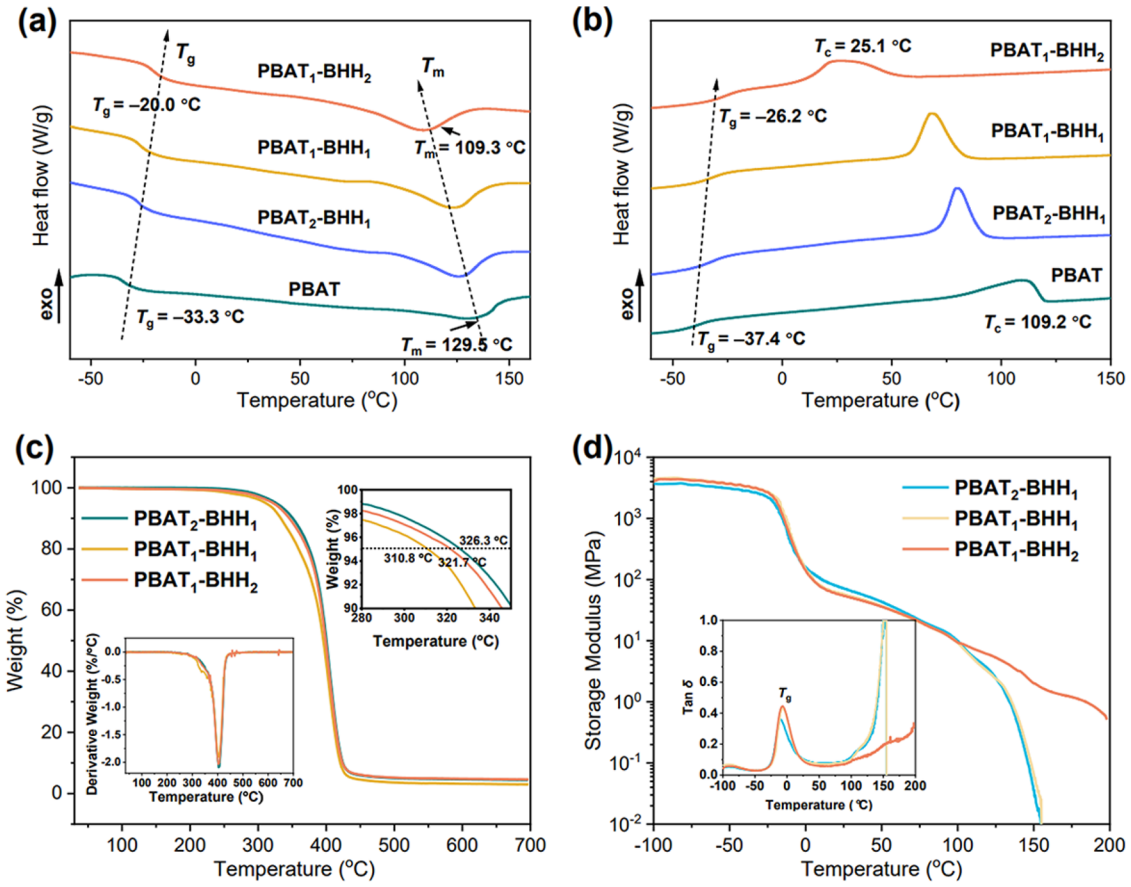

Figure 3. DSC curves (a) during the second heating and (b) during the first cooling of PBAT and PBAT$_x$-BHH$_y$ and (c) TGA and (d) DTG curves of PBAT$_x$-BHH$_y$.

dramatically from 34% of PBAT to 70−80% of PBAT$_x$-BHH$_y$ (Figure S5). The scattered multiple hydrogen bonding interaction of the BHH and PDI hard segments and the hierarchical nanostructure are illustrated in Figure 1b,c.

The thermal properties of PBAT-BHH samples were examined by DSC, thermogravimetric analysis (TGA), and dynamic mechanical analysis (DMA). DSC measurements (Figure 3a) demonstrate that the glass transition temperatures (T_g) of PBAT$_x$-BHH$_y$ increased gradually from −33.3 to −20.0 °C with the increase in BHH content, while the melting point (T_m) exhibited a decreasing trend from 129.5 to 109.3 °C. The cooling curves (Figure 3b) indicate that the crystallization temperature (T_c) of PBAT$_x$-BHH$_y$ decreased from 109.2 to 25.1 °C. The crystallinity of PBAT$_x$-BHH$_y$ calculated from enthalpy (Table S2) also decreased significantly compared to the raw PBAT during the same thermal process. The increase in T_g and the decrease in T_m, T_c, and crystallinity confirm that the multiple hydrogen bonding interaction brought by BHH inhibits the molecular chain motility and hinders the crystallization of PBAT, which conversely proves that a large number of hydrogen bonds can increase the intermolecular chain force to achieve high mechanical strength. All PBAT-BHH samples display thermal decomposition temperatures of >310 °C ($T_{d,5\%}$, the temperature of 5% mass loss from TGA analysis) with a single decomposition peak in the differential curve (Figure 3c). The materials showed a homogeneous system without stepwise decomposition, which also verified the successful chemical copolymerization other than physical blending.[43]

Dynamic mechanical analysis (DMA, Figure 3d) of PBAT$_x$-BHH$_y$ further demonstrates that all PBAT$_x$-BHH$_y$ present only one T_g from −6.6 to −11.2 °C in the curves of tangent loss factor (tan δ), higher than the T_g value measured by DSC, presumably due to the thermal hysteresis of the DMA instrument. In the storage modulus (E') curves, the E' value decreased rapidly at T_g, presented a slow decrease rate after T_g, and then decreased rapidly again after 100 °C, resulting from the melting of the PBAT crystals. The E' of PBAT$_2$-BHH$_1$ and PBAT$_1$-BHH$_1$ continued to decrease rapidly, reaching a maximum rate after 125 °C until the sample flowed and the test was automatically terminated at 155 °C. In particular, PBAT$_1$-BHH$_2$ showed a slow modulus decreasing behavior above the melting temperature and did not show any flow phenomenon up to 200 °C. This could be attributed to the higher hydrogen bonding density in PBAT$_1$-BHH$_2$, resulting in stronger and tighter molecular interaction.

We evaluated the mechanical properties of the obtained PBAT$_x$-BHH$_y$ with different mole ratios of PBAT and BHH by tensile tests. The typical stress−strain curves are shown in Figure 4a and Figure S6, and the specific performances are recorded in Tables S3−S6. All PBAT$_x$-BHH$_y$ exhibit the elastic stage, yield point, and strain hardening stages, and strain hardening appears immediately after yielding without necking and develops in a fairly homogeneous manner. Compared to the PBAT raw material, the tensile strength and the toughness of PBAT$_x$-BHH$_y$ presented a remarkable enhancement in line with our estimate (Figure 4b). PBAT$_2$-BHH$_1$ with PABT:BHH at 2:1 (mass ratio of PBAT, w_{PBAT}, ∼96%) presented a tensile

https://doi.org/10.1021/acs.macromol.4c01153
Macromolecules 2024, 57, 7043−7051

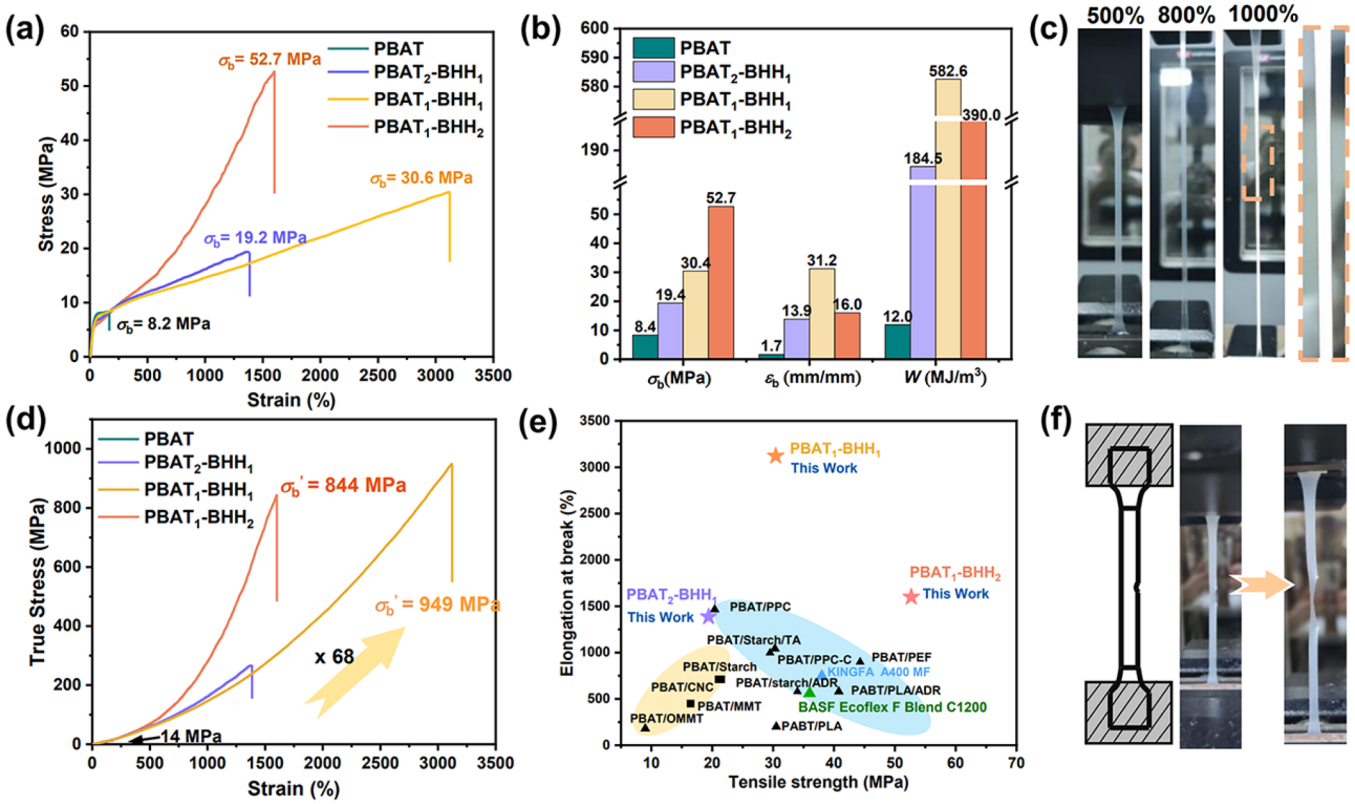

Figure 4. (a) Stress−strain curve, (b) comparison of mechanical properties including tensile strength (σ), Young's modulus (E), elongation at break (ε), and fracture toughness (W) of PBAT$_x$-BHH$_y$ compared with parent PBAT, (c) photograph of PBAT$_1$-BHH$_1$ at different stretching strains, (d) true stress−strain curve of PBAT$_x$-BHH$_y$ and PBAT, (e) comparison of the mechanical properties of PBAT$_x$-BHH$_y$ in this study and commercial PBAT, PBAT/nanofiller composites,[29−31] and PBAT/other polymer blends[11,23−28] reported in the references, and (f) photograph of tear resistance.

strength (σ_b) of 19 MPa and an elongation at break (ε_b) of 1380%. With the increase in BHH content, PBAT$_1$-BHH$_1$ ($w_{PBAT} \sim 94\%$) presented $\sigma_b \sim 30.6$ MPa and $\varepsilon_b \sim 3000\%$, and the fracture toughness reached 583 MJ/m^3. When the BHH mole ratio further increased, the tensile strength of PBAT$_1$-BHH$_2$ ($w_{PBAT} \sim 90\%$) increased high up to 52.7 MPa, while the elongation at break declined but was still higher than 1500%. Indeed, no obvious deterioration occurred in Young's modulus (Tables S3−S6), which did not affect the requirements for its use as packaging plastics or other applications. We observed significant changes in transparency and stress whitening effects after strain at ∼1000% during stretching (Figure 4c), i.e., the specimen changed from translucent to opaque as the strain increased to be higher than 800%, which should correspond to stress-induced crystallization and silver streak effects. The true stress values of PBAT$_1$-BHH$_1$ and PBAT$_1$-BHH$_2$ reached 949 and 844 MPa, respectively, which were more than 60 times of the PBAT feedstock ∼14 MPa (Figure 4d).

The overall performance of PBAT-BHH prepared by this strategy is at the top of and even much better than the existing reports on PBAT composites blended with nanoparticles and strong polymers (Figure 4e).[11,23−31] Although some of the reported tensile strengths or elongations at break of the PBAT blending systems are comparable to those in our work, our PBAT$_x$-BHH$_y$ materials present both excellent high strength and toughness, and the mechanical properties can be tailored by feasibly adjusting the hydrogen bonding segment content. The Greensmith method was conducted to assess the tear resistance of PBAT-BHH (Figure 4f). It was found that with the increase in BHH mole ratio, the tear resistance greatly increased. The fracture energies (G_c) of PBAT$_2$-BHH$_1$, PBAT$_1$-BHH$_1$, and PBAT$_1$-BHH$_2$ were 26.6, 60.1, and 122.9 kJ/m^2 (Figure S7), respectively. This indicates that the hydrogen bonding interaction also improves the tear resistance of the materials.

To understand the excellent mechanical performance of PBAT$_x$-BHH$_y$, we performed in situ wide-angle X-ray diffraction (WAXD) tests (Figure 5a−c) to reveal the microphase structures before and during the stretching process. Before stretching, all PBAT-BHH displayed five diffraction halos with low peak intensity at 2θ of 16.3°, 17.7°, 20.5°, 23.4°, and 25.3° corresponding to five planes (011), (010), (110), (100), and (111) of PBAT crystals, respectively.[18,44] The higher the content of BHH, the lower the scattering intensity, consistent with the deterioration of BHH on the crystallization of PBAT. After stretching, the diffraction intensity of the crystalline peaks at (010) (17.5−18.5°) and (100) crystal facets (22.9−23.5°) was significantly enhanced, while those at (011) and (111) crystal facets decreased and even disappeared for PBAT-BHH, which demonstrated strain-induced crystallization because of the preferential orientation of polymer chains along the stretching direction.[44] In addition to the intensity variations, the centered peak position of the (010) facet shifted to a higher 2θ value, but that of the (100) facet shifted to a lower 2θ value, which originated from orientation, distortion, and form transition of the crystals during stretching. 2D WAXD profiles (Figure 5d) presented

https://doi.org/10.1021/acs.macromol.4c01153
Macromolecules 2024, 57, 7043−7051

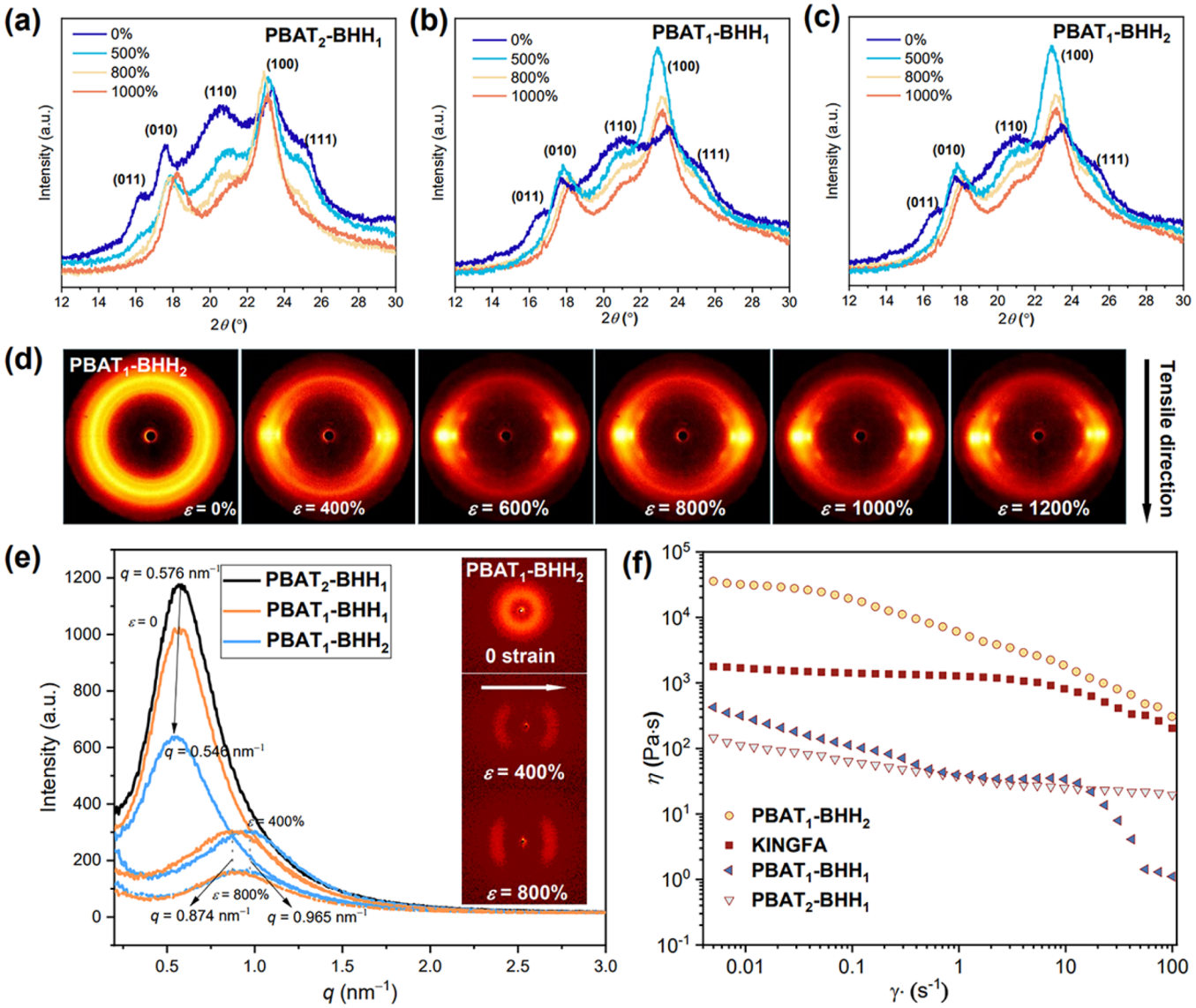

Figure 5. WAXD spectra of (a–c) PBAT$_x$-BHH$_y$ before and after stretching with different strains, (d) 2D-WAXD patterns of PBAT$_1$-BHH$_2$ with indicated strain, (e) 1D-SAXS of PBAT$_x$-BHH$_y$ before and after stretching with the 2D-SAXS patterns of PBAT$_1$-BHH$_2$ inserted, and (f) apparent viscosity–shear rate curves of PBAT$_x$-BHH$_y$ compared with high-MW PBAT from KINGFA.

reflection rings before stretching and became an oblate shape with strong reflection spots concentrated in the equatorial direction after stretching (perpendicular to the stretching direction), further indicating the orientation of lamellar PBAT crystals. The (100) diffraction intensity of PBAT$_1$-BHH$_2$ (Figure 5c) changes the largest after stretching, illustrating that the strong H-bonding interaction and low initial crystalline state give rise to the stronger strain-induced crystallization effect for the best improvement of the mechanical properties.

The small-angle X-ray scattering (SAXS) experiments were performed to further reveal the microstructure of PBAT-BHH (Figure 5e). Before stretching, a wide scattering peak with the centered q value at 0.54–0.57 nm^{-1} occurred in three PBAT$_x$-BHH$_y$. After stretching, the scattering peak shifted to the high q value direction at q = 0.87–0.96 nm^{-1}, and the scattering halo separated into two arcs along the elongation direction, indicating that this scattering mainly originates from the lamellar stacking of PBAT crystals because of the electron density contrast between the crystalline and amorphous PBAT. The q value increase means the decrease in the period size, consistent with the creation of more tiny crystalline domains during stretching. It is worth noting that the phase separation between urethane hard segments and PBAT segments should also exist in the materials, although the diffraction was weak because of the low electron density difference and the low content of the hard segment, yet the effective hydrogen interaction of the hard segments had been demonstrated by FT-IR (Figure 2d). Therefore, the hierarchical phase-separated nanostructures, stress-induced recrystallization behavior, and the energy dissipation of the hydrogen bonding arrays together contribute to the high strength and toughness of PBAT$_x$-BHH$_y$.

Finally, the rheological measurements yielded an apparent viscosity–shear rate curve (Figure 5d) to qualify the processing ability. As seen in Figure 5d, PBAT$_1$-BHH$_1$ and PBAT$_2$-BHH$_1$ exhibited lower apparent viscosities than commercial PBAT products (KINGFA ECOPOND A400 MF), especially in the high shear rate region (10–100 s^{-1}),

https://doi.org/10.1021/acs.macromol.4c01153
Macromolecules 2024, 57, 7043–7051

where the viscosity was less than 100 Pa·s. Although $PBAT_1$-BHH_2 showed higher apparent viscosity compared to the commercial PBAT when the measured shear rates were less than 10 s^{-1}, it still exhibited comparable viscosity in the high shear rate region (10 to 100 s^{-1}). Therefore, PBAT-BHH displays highly enhanced mechanical performances with good processing ability for producing commercial commodities. Moreover, the low-content (<10 wt %) biobased and CO_2-derived chain extenders ensure the sustainability and biodegradability.

CONCLUSIONS

In summary, this study demonstrates that multiple hydrogen bonding units can be incorporated into biodegradable PBAT to enhance the strength and toughness through feasible melting copolymerization using CO_2-derived and biobased chain extenders. Due to the similar melting temperature of the hydrogen bonding monomer compared to PBAT, the melting chain extension reaction was uniform. The synthesized PBAT-BHH materials with the mass ratio of PBAT higher than 90% show highly enhanced strength and toughness without deterioration of processing ability. In addition, the synthesis route allows for facile adjustment of the content of the BHH hydrogen bonding units, enabling customization of its mechanical properties to meet the requirements of specific applications. The mechanical strength and toughness ($\delta_b \sim 30$ MPa, $\varepsilon_b \sim 3000\%$; $\delta_b \sim 52$ MPa, $\varepsilon_b \sim 1500\%$) reach a much better level than those of conventional high molecular-weighted PBAT and its composites. The approach described in this study highlights a potentially scalable chain extension method from commercially available low-molecular-weight PBAT to incorporate multiple hydrogen bonding interaction units that break through the performance limit of biodegradable polyester to further replace polyolefin materials.

ASSOCIATED CONTENT

Supporting Information

The Supporting Information is available free of charge at https://pubs.acs.org/doi/10.1021/acs.macromol.4c01153.

Materials, synthesis and characterization method of BHH and PBAT-BHH, additional ^{1}H NMR spectra, FT-IR spectra, and tensile curves of PBAT-BHH and notched samples, and additional tables of the DSC, GPC, and tensile measurement results (PDF)

AUTHOR INFORMATION

Corresponding Authors

Ling-Ying Shi − *College of Polymer Science and Engineering, State Key Laboratory of Polymer Materials Engineering, Sichuan University, Chengdu 610065, China;* orcid.org/0000-0002-6620-7878; Email: shilingying@scu.edu.cn

Ke-Ke Yang − *The Collaborative Innovation Center for Eco-Friendly and Fire-Safety Polymeric Materials (MoE), National Engineering Laboratory of Eco-Friendly Polymeric Materials (Sichuan), State Key Laboratory of Polymer Materials Engineering, College of Chemistry, Sichuan University, Chengdu 610064, China;* orcid.org/0000-0002-7019-6059; Email: kkyang@scu.edu.cn

Yu-Zhong Wang − *The Collaborative Innovation Center for Eco-Friendly and Fire-Safety Polymeric Materials (MoE), National Engineering Laboratory of Eco-Friendly Polymeric Materials (Sichuan), State Key Laboratory of Polymer Materials Engineering, College of Chemistry, Sichuan University, Chengdu 610064, China*; Email: polymers@vip.126.com

Authors

Zhi-Xiong Fei − *College of Polymer Science and Engineering, State Key Laboratory of Polymer Materials Engineering, Sichuan University, Chengdu 610065, China*

Jingrui Sun − *College of Polymer Science and Engineering, State Key Laboratory of Polymer Materials Engineering, Sichuan University, Chengdu 610065, China*

Chang Cui − *College of Polymer Science and Engineering, State Key Laboratory of Polymer Materials Engineering, Sichuan University, Chengdu 610065, China*

Chenxiao Yin − *College of Polymer Science and Engineering, State Key Laboratory of Polymer Materials Engineering, Sichuan University, Chengdu 610065, China*

Rui Zhan − *The Collaborative Innovation Center for Eco-Friendly and Fire-Safety Polymeric Materials (MoE), National Engineering Laboratory of Eco-Friendly Polymeric Materials (Sichuan), State Key Laboratory of Polymer Materials Engineering, College of Chemistry, Sichuan University, Chengdu 610064, China*

Complete contact information is available at: https://pubs.acs.org/10.1021/acs.macromol.4c01153

Author Contributions

[§]Z.-X.F. and J.S. contributed equally to this work.

Notes

The authors declare no competing financial interest.

ACKNOWLEDGMENTS

Financial supports from the National Key Research and Development Program of China (project no. 2022YFC2104600) and National Natural Science Foundation of China (grant 52273024) are gratefully acknowledged.

REFERENCES

(1) Geyer, R.; Jambeck, J. R.; Law, K. L. Production, use, and fate of all plastics ever made. *Sci. Adv.* **2017**, *3* (7), No. e1700782.

(2) MacLeod, M.; Arp, H. P. H.; Tekman, M. B.; Jahnke, A. The global threat from plastic pollution. *Science* **2021**, *373* (6550), 61−65.

(3) Shi, C.; Rorrer, N. A.; Shaw, A. L.; Clarke, R. W.; Buss, B. L.; Beckham, G. T.; Broadbelt, L. J.; Chen, E. Y. X. Topology-Accelerated and Selective Cascade Depolymerization of Architecturally Complex Polyesters. *J. Am. Chem. Soc.* **2024**, *146* (13), 9261−9271.

(4) Jehanno, C.; Alty, J. W.; Roosen, M.; De Meester, S.; Dove, A. P.; Chen, E. Y. X.; Leibfarth, F. A.; Sardon, H. Critical advances and future opportunities in upcycling commodity polymers. *Nature* **2022**, *603* (7903), 803−814.

(5) Fan, L.-X.; Chen, L.; Zhang, H.-Y.; Xu, W.-H.; Wang, X.-L.; Xu, S.; Wang, Y.-Z. Dual Photo-Responsive Diphenylacetylene Enables PET In-Situ Upcycling with Reverse Enhanced UV-Resistance and Strength. *Angew. Chem., Int. Ed.* **2023**, *62* (52), No. e202314448.

(6) Albertsson, A.-C.; Hakkarainen, M. Designed to degrade. *Science* **2017**, *358* (6365), 872−873.

(7) Tu, Y.-M.; Wang, X.-M.; Yang, X.; Fan, H.-Z.; Gong, F.-L.; Cai, Z.; Zhu, J.-B. Biobased High-Performance Aromatic−Aliphatic Polyesters with Complete Recyclability. *J. Am. Chem. Soc.* **2021**, *143* (49), 20591−20597.

(8) Worch, J. C.; Dove, A. P. 100th Anniversary of Macromolecular Science Viewpoint: Toward Catalytic Chemical Recycling of Waste (and Future) Plastics. *ACS Macro Lett.* **2020**, *9* (11), 1494−1506.

(9) Shi, C.; Quinn, E. C.; Diment, W. T.; Chen, E. Y. X. Recyclable and (Bio)degradable Polyesters in a Circular Plastics Economy. *Chem. Rev.* **2024**, *124* (7), 4393−4478.
(10) Witt, U.; Einig, T.; Yamamoto, M.; Kleeberg, I.; Deckwer, W. D.; Müller, R. J. Biodegradation of aliphatic−aromatic copolyesters: evaluation of the final biodegradability and ecotoxicological impact of degradation intermediates. *Chemosphere* **2001**, *44* (2), 289−299.
(11) Jiang, L.; Wolcott, M. P.; Zhang, J. Study of Biodegradable Polylactide/Poly(butylene adipate-co-terephthalate) Blends. *Biomacromolecules* **2006**, *7* (1), 199−207.
(12) Deng, S.; Bai, H.; Liu, Z.; Zhang, Q.; Fu, Q. Toward Supertough and Heat-Resistant Stereocomplex-Type Polylactide/Elastomer Blends with Impressive Melt Stability via in Situ Formation of Graft Copolymer during One-Pot Reactive Melt Blending. *Macromolecules* **2019**, *52* (4), 1718−1730.
(13) Li, Y.; Xin, R.; Wang, S.; Guo, Z.; Sun, X.; Ren, Z.; Li, H.; Li, L.; Yan, S. Structure and Mechanical Property of Melt-Drawn Oriented PLA Ultrathin Films. *Macromolecules* **2021**, *54* (19), 9124−9134.
(14) Barletta, M.; Aversa, C.; Ayyoob, M.; Gisario, A.; Hamad, K.; Mehrpouya, M.; Vahabi, H. Poly(butylene succinate) (PBS): Materials, processing, and industrial applications. *Prog. Polym. Sci.* **2022**, *132*, No. 101579.
(15) Jian, J.; Xiangbin, Z.; Xianbo, H. An overview on synthesis, properties and applications of poly(butylene-adipate-co-terephthalate)−PBAT. *Adv. Ind. Eng. Polym.* **2020**, *3* (1), 19−26.
(16) Yang, Y.; Min, J.; Xue, T.; Jiang, P.; Liu, X.; Peng, R.; Huang, J.-W.; Qu, Y.; Li, X.; Ma, N.; Tsai, F.-C.; Dai, L.; Zhang, Q.; Liu, Y.; Chen, C.-C.; Guo, R.-T. Complete bio-degradation of poly(butylene adipate-co-terephthalate) via engineered cutinases. *Nat. Commun.* **2023**, *14* (1), 1645.
(17) Siegenthaler, K. O.; Agari, M.; Auffermann, J.; Barth, M. P.; Battagliarin, G.; Künkel, A.; Lauer, F.; Lohmann, J.; Nabifar, A.; Yamamoto, M., ecoflex® and ecovio®: Biodegradable, Performance-Enabling Plastics. In *Synthetic Biodegradable and Biobased Polymers: Industrial Aspects and Technical Products*, Künkel, A.; Battagliarin, G.; Winnacker, M.; Rieger, B.; Coates, G., Eds. Springer International Publishing: Cham, 2024; pp 111−175.
(18) Fukushima, K.; Wu, M.-H.; Bocchini, S.; Rasyida, A.; Yang, M.-C. PBAT based nanocomposites for medical and industrial applications. *Mater. Sci. Eng., C* **2012**, *32* (6), 1331−1351.
(19) Xu, Z.; Zheng, B.; Yang, Y.; Yang, Y.; Jiang, G.; Tian, Y. Effects of biodegradable (PBAT/PLA) and conventional (LDPE) mulch film residues on bacterial communities and metabolic functions in different agricultural soils. *J. Hazard. Mater.* **2024**, *472*, No. 134425.
(20) Moustafa, H.; El Kissi, N.; Abou-Kandil, A. I.; Abdel-Aziz, M. S.; Dufresne, A. PLA/PBAT Bionanocomposites with Antimicrobial Natural Rosin for Green Packaging. *ACS Appl. Mater. Interfaces* **2017**, *9* (23), 20132−20141.
(21) Fu, Y.; Wu, G.; Bian, X.; Zeng, J.; Weng, Y. Biodegradation Behavior of Poly(Butylene Adipate-Co-Terephthalate) (PBAT), Poly(Lactic Acid) (PLA), and Their Blend in Freshwater with Sediment. *Molecules* **2020**, *25* (17), 3946.
(22) Zhao, J.; Li, X.; Pan, H.; Ai, X.; Yang, H.; Zhang, H.; Gao, G.; Dong, L. Rheological, thermal and mechanical properties of biodegradable poly(lactic acid)/poly(butylene adipate-co-terephthalate)/poly(propylene carbonate) polyurethane trinary blown films. *Polym. Bull.* **2020**, *77* (8), 4235−4258.
(23) Wang, X.; Peng, S.; Chen, H.; Yu, X.; Zhao, X. Mechanical properties, rheological behaviors, and phase morphologies of high-toughness PLA/PBAT blends by in-situ reactive compatibilization. *Compos. Part B-Eng.* **2019**, *173*, No. 107028.
(24) Jiang, G.; Wang, F.; Zhang, S.; Huang, H. Structure and improved properties of PPC/PBAT blends via controlling phase morphology based on melt viscosity. *J. Appl. Polym. Sci.* **2020**, *137* (31), 48924.
(25) Gao, F.-X.; Cai, Y.; Liu, S.-J.; Wang, X.-H. High-Performance Biodegradable PBAT/PPC Composite Film Through Reactive Compatibilizer. *Chin. J. Polym. Sci.* **2023**, *41* (7), 1051−1058.
(26) Wang, B.; Wei, C.; Li, C.; Sang, L.; Wang, L.; Wei, Z.; Qi, M. Incorporation of Poly(ethylene 2,5-furanoate) into Poly(butylene adipate-co-terephthalate) toward Sustainable Food Packaging Films with Enhanced Strength and Barrier Properties. *ACS Sustain. Chem. Eng.* **2023**, *11* (2), 597−606.
(27) Fourati, Y.; Tarrés, Q.; Mutjé, P.; Boufi, S. PBAT/thermoplastic starch blends: Effect of compatibilizers on the rheological, mechanical and morphological properties. *Carbohydr. Polym.* **2018**, *199*, 51−57.
(28) Zhang, S.; Lin, Z.; Li, J.; Jiang, G.; Hu, C. Elevated ductility, optical, and air barrier properties of poly (butyleneadipate-co-terephthalate) bio-based films via novel thermoplastic starch feature. *Polym. Adv. Technol.* **2019**, *30* (4), 852−862.
(29) Pinheiro, I. F.; Ferreira, F. V.; Souza, D. H. S.; Gouveia, R. F.; Lona, L. M. F.; Morales, A. R.; Mei, L. H. I. Mechanical, rheological and degradation properties of PBAT nanocomposites reinforced by functionalized cellulose nanocrystals. *Eur. Polym. J.* **2017**, *97*, 356−365.
(30) Chivrac, F.; Kadlecová, Z.; Pollet, E.; Avérous, L. Aromatic Copolyester-based Nano-biocomposites: Elaboration, Structural Characterization and Properties. *J. Polym. Environ.* **2006**, *14* (4), 393−401.
(31) Chen, J.-H.; Yang, M.-C. Preparation and characterization of nanocomposite of maleated poly(butylene adipate-co-terephthalate) with organoclay. *Mater. Sci. Eng., C* **2015**, *46*, 301−308.
(32) Lee, S.-M.; Pippel, E.; Gösele, U.; Dresbach, C.; Qin, Y.; Chandran, C. V.; Bräuniger, T.; Hause, G.; Knez, M. Greatly Increased Toughness of Infiltrated Spider Silk. *Science* **2009**, *324* (5926), 488−492.
(33) Keten, S.; Xu, Z.; Ihle, B.; Buehler, M. J. Nanoconfinement controls stiffness, strength and mechanical toughness of β-sheet crystals in silk. *Nat. Mater.* **2010**, *9* (4), 359−367.
(34) Yan, X.; Liu, Z.; Zhang, Q.; Lopez, J.; Wang, H.; Wu, H.-C.; Niu, S.; Yan, H.; Wang, S.; Lei, T.; Li, J.; Qi, D.; Huang, P.; Huang, J.; Zhang, Y.; Wang, Y.; Li, G.; Tok, J. B. H.; Chen, X.; Bao, Z. Quadruple H-Bonding Cross-Linked Supramolecular Polymeric Materials as Substrates for Stretchable, Antitearing, and Self-Healable Thin Film Electrodes. *J. Am. Chem. Soc.* **2018**, *140* (15), 5280−5289.
(35) Yang, K.; Li, Q.; Tian, S.; Wang, J.; Lu, G.; Guo, H.; Xu, S.; Zhang, L.; Yang, J. Highly Stretchable, Self-Healing, and Sensitive E-Skins at − 78 °C for Polar Exploration. *J. Am. Chem. Soc.* **2024**, *146* (15), 10699−10707.
(36) Yao, Y.; Xu, Z.; Liu, B.; Xiao, M.; Yang, J.; Liu, W. Multiple H-Bonding Chain Extender-Based Ultrastiff Thermoplastic Polyurethanes with Autonomous Self-Healability, Solvent-Free Adhesiveness, and AIE Fluorescence. *Adv. Funct. Mater.* **2021**, *31* (4), No. 2006944.
(37) Guo, Z.; Lu, X.; Wang, X.; Li, X.; Li, J.; Sun, J. Engineering of Chain Rigidity and Hydrogen Bond Cross-Linking toward Ultra-Strong, Healable, Recyclable, and Water-Resistant Elastomers. *Adv. Mater.* **2023**, *35* (21), No. 2300286.
(38) Sijbesma, R. P.; Beijer, F. H.; Brunsveld, L.; Folmer, B. J. B.; Hirschberg, J. H. K. K.; Lange, R. F. M.; Lowe, J. K. L.; Meijer, E. W. Reversible Polymers Formed from Self-Complementary Monomers Using Quadruple Hydrogen Bonding. *Science* **1997**, *278* (5343), 1601−1604.
(39) Deng, Y.; Li, S.; Zhao, J.; Zhang, Z.; Zhang, J.; Yang, W. Crystallizable and tough aliphatic thermoplastic poly(ether urethane)s synthesized through a non-isocyanate route. *RSC Adv.* **2014**, *4* (82), 43406−43414.
(40) Wołosz, D.; Parzuchowski, P. G.; Rolińska, K. Environmentally Friendly Synthesis of Urea-Free Poly(carbonate-urethane) Elastomers. *Macromolecules* **2022**, *55* (12), 4995−5008.
(41) Sun, H.; Fang, X.; Zhu, Y.; Yu, Z.; Lu, X.; Sun, J. Highly tough, degradable, and water-resistant bio-based supramolecular plastics comprised of cellulose and tannic acid. *J. Mater. Chem. A* **2023**, *11*, 7193−7200.
(42) Fang, X.; Tian, N.; Hu, W.; Qing, Y.; Wang, H.; Gao, X.; Qin, Y.; Sun, J. Dynamically Cross-Linking Soybean Oil and Low-

https://doi.org/10.1021/acs.macromol.4c01153
Macromolecules 2024, 57, 7043−7051

Molecular-Weight Polylactic Acid toward Mechanically Robust, Degradable, and Recyclable Supramolecular Plastics. *Adv. Funct. Mater.* **2022**, *32*, No. 2208623.

(43) Wang, H.-H.; Zhou, S.-J.; Xiong, S.-J.; Liu, Q.; Tian, H.; Yu, S.; Yuan, T.-Q. High-performance thermoplastic starch/poly(butylene adipate-co-terephthalate) blends through synergistic plasticization of epoxidized soybean oil and glycerol. *Int. J. Biol. Macromol.* **2023**, *242*, No. 124716.

(44) Zhou, J.; Zheng, Y.; Shan, G.; Bao, Y.; Wang, W.; Pan, P. Stretch-Induced α-to-β Crystal Transition and Lamellae Structural Evolution of Poly(butylene adipate-ran-terephthalate) Aliphatic−Aromatic Copolyester. *Macromolecules* **2019**, *52* (3), 1334−1347.

https://doi.org/10.1021/acs.macromol.4c01153
Macromolecules 2024, 57, 7043−7051